Interference microscopy for three-dimensional imaging with wavelength-to-depth encoding

Guoqiang Li, Pang-Chen Sun, Paul C. Lin, and Yeshayahu Fainman

Department of Electrical and Computer Engineering, University of California, San Diego, La Jolla, California 92093-0407

Received May 31, 2000

A novel interference microscope for three-dimensional (3D) imaging based on a wavelength-to-depth encoding technique is presented. Wavelength-to-depth encoding is realized by use of a diffractive lens and wavelength tuning. A high depth resolution of 0.71 μm is obtained with 0.90-N.A. objective lenses. Experimental measurements of a four-level grating are presented, and the results are found to be comparable with those obtained with a Dektak profilometer and a similar interference microscope that uses mechanical depth scanning. The system is promising for fast, noncontact, high-resolution 3D imaging. © 2000 Optical Society of America

OCIS codes: 110.6880, 120.4290, 170.1650, 180.3170.

High-resolution noncontact three-dimensional (3D) optical imaging techniques are very attractive for many applications; in particular, the confocal imaging[1–3] technique has been intensively studied. A different approach, called interference microscopy,[4–11] can eliminate the need for lateral scanning. In this scheme depth information is obtained by measurement of the degree of coherence between corresponding pixels in the object and the reference planes. This scheme uses the entire available illumination and measures all the transverse points in parallel. In addition, it is capable of the same transverse resolution and depth response as a confocal microscope.[4,5] Different types of architecture based on the Linnik microscope,[4] the Mirau correlation microscope,[5,6] and the Michelson interferometer[7–11] have been proposed. In these systems the object is scanned along the vertical axis (z axis) by a piezoelectric translation stage. In this Letter we propose an interferometric microscope for 3D imaging that avoids mechanical depth scanning by introduction of a wavelength-to-depth encoding technique. Wavelength-to-depth encoding is realized by use of a diffractive lens combined with a wavelength-tunable laser. This construction results in a novel interferometric microscope architecture in which separate diffractive and refractive imaging systems are used in the object and the reference arms, respectively. High-resolution 3D profiles of the object can be obtained after calibration of the wavelength-to-depth encoding and measurement of the coherence function for each image pixel. The experimental results obtained are found to be in good agreement with those measured with a Dektak profilometer and a similar interference microscope system that uses mechanical scanning.

A schematic diagram of our interference microscope setup is shown in Fig. 1. In the proof-of-principle experiment, linearly polarized quasi-monochromatic light from a wavlength-tunable Ti:sapphire laser is used. The collimated beam is transmitted through rotating ground glass, which generates a spatially incoherent optical field. The coherence characteristic of a spatially incoherent source can be described by the mutual intensity function[12] and calculated by means of the Van Cittert–Zernike theorem. The coherence area is defined such that the light from any two points within the coherence area will interfere. Assuming that the size of the coherence area in plane x_1y_1 is so small that its optical field can be approximated by a δ-function distribution, we can term each basic area a coherence cell. In Fig. 1, two sets of coherence cells are created in the two arms by the beam splitter. Any coherence cell in one arm will be coherent with one and only one coherent cell in the other arm. If the two corresponding coherence cells directly overlap in image space, high-contrast inference fringes will be observed. In the object arm we employ a 4-f imaging system consisting of a diffractive lens (L_1) and an objective lens (L_2) to image inversely the coherent cells in plane x_1y_1 to the object plane, with x_1y_1 being the focal plane of the diffractive lens for the center wavelength λ_c of our system. Another 4-f imaging system consisting of a refractive, large-aperture achromatic lens (L_3) and an objective lens (L_4) is adopted in the reference arm. The coherent cells in the object plane and the reference mirror are imaged back to plane x_5y_5. The overlapping optical fields are imaged through lens (L_5) onto the CCD,

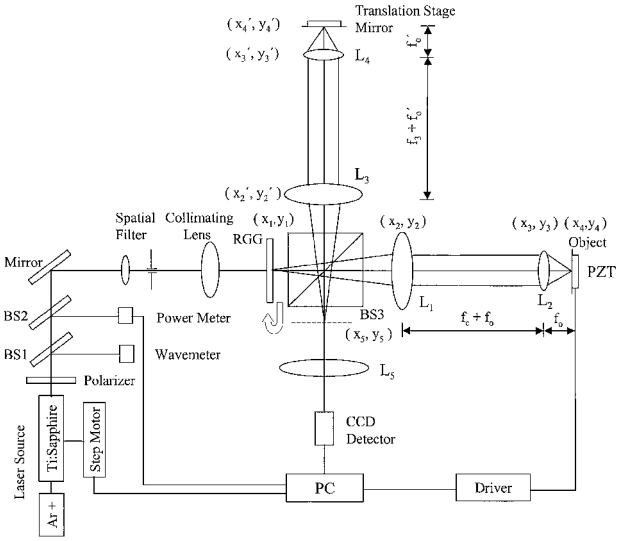

Fig. 1. Schematic diagram of the interference microscope using wavelength-to-depth encoding. BS1–BS3, beam splitters; RGG, rotating ground glass. See text for other definitions.

0146-9592/00/201505-03$15.00/0

where the interference patterns are detected and recorded.

For the first-order diffraction, the focal length of the diffractive lens changes linearly with respect to the operating wavelength.[13] Suppose that the object arm is aligned for a center wavelength $\lambda_c = 863$ nm. The corresponding focal length of the diffractive lens is f_c, and the coherent cells in plane x_1y_1 are imaged to the plane with an image distance f_o, where f_o is the focal length of the objective lens. When the operating wavelength is tuned away from λ_c by $\Delta\lambda$, there will be a corresponding focal-length change Δf of diffractive lens L_1, and consequently the coherent cells in plane x_1y_1 will be imaged to the plane with an image distance $f_o + \Delta z$. If $f_c \gg \Delta f$, the displacement Δz can be approximated as

$$\Delta z = \left(\frac{f_0}{f_c}\right)^2 \Delta f = -\left(\frac{f_0}{f_c}\right)^2 \frac{f(\lambda_d)}{\lambda_d}\,\Delta\lambda\,. \qquad (1)$$

If we put a reflection mirror in the back focal plane of the objective lens, the optical field that is incident upon the mirror and the field that is incident upon plane x_5y_5 will change with a change of wavelength. According to Fourier optics,[14] the optical field distribution in plane x_4y_4 is the point-spread function of the first subsystem (from plane x_1y_1 to plane x_4y_4), and the total impulse in plane x_5y_5 is the ideal geometric image of $U_4(x, y)$ convolved with the point-spread function of the second subsystem (from plane x_4y_4 to plane x_5y_5). For each subsystem the point-spread function is the Fourier transform of its general pupil function, which is the physical exit pupil multiplied by a quadratic phase function. This quadratic phase function can be considered a wave aberration that is due to defocusing when the operating wavelength is tuned away from central wavelength λ_c.

In the reference arm, if we assume the chromatic aberrations to be negligible, there is no wave aberration owing to defocusing for different operating wavelengths. The correlation of the two optical fields from the object and the reference arms will vary with the wavelength. Generally speaking, the correlation signal is sinusoidal, with a fairly constant frequency modulated by an envelope function. This envelope represents the coherence between the two signals from the object and the reference arms. Assuming that the maximum optical path difference between the two waves is much smaller than the coherence length of the laser, we note that the correlation function between the two waves can be represented by the mutual intensity, and the coherence degree factor can be expressed by the modulus of the mutual intensity. It can be seen that the maximum coherence degree factor occurs at the wavelength at which the mirror is placed in the exact image plane of the point source. If the mirror is moved out of this plane, the maximum coherence factor will occur at another wavelength, thus permitting wavelength-to-depth encoding. If the encoding is calibrated, this technique can be used to perform 3D profilometry.

To calibrate the wavelength-to-depth encoding we use a flat mirror as the object. This mirror is driven along the longitudinal axis by a piezoelectric transducer (PZT). In each step the piezoelectric transducer moves 0.1 μm. The wavelength of the laser is monitored by a wavemeter with a sensitivity of ± 0.02 nm. A powermeter is also used to monitor the power in real time. The two 100× objective lenses (NPL Fluotar, Leitz Wetzlar) have a N.A. of 0.90. At a given wavelength, e.g., $\lambda_1 = 830$ nm, the interference fringes at one point (x, y) are recorded as the object mirror is scanned in the z direction. We demodulate the fringes to find the center of mass of the envelope and the corresponding $z_1(x, y)$. This location is the focal-point position of point (x, y) at λ_1. Then, we increase the wavelength to λ_2, repeat the operation, and obtain the focal position $z_2(x, y)$ of the same transverse point at λ_2, and so on. In our case the wavelength is tuned from 830 to 894 nm, in increments of 2 nm. Figure 2 shows the calibration plot of the depth position (longitudinal focal position) of one pixel versus wavelength. By a linear curve fit of the result, the expression for $z(\lambda)$ of this pixel can be obtained as $z(\mu\text{m}) = 0.04216\lambda(\text{nm}) - 23.64$. For 3D imaging, we are concerned only with the slope of the linear curve. Owing to the aberrations that exist in the imaging lenses, there may be very small variations among the slopes obtained at different pixels. By averaging of the values of the slope for pixels in a certain area, the factor for wavelength-to-depth encoding is found to be $\Delta z/\Delta\lambda = 0.04249$ μm/nm. According to Eq. (1), the sensitivity of the system depends on the demagnification power $[(f_0/f_c)^2]$ of the 4-f imaging system and the dispersion strength $[f(\lambda_d)/\lambda_d]$ of the diffractive lens.

To measure the depth discrimination with wavelength-to-depth encoding we fix the object mirror and tune the wavelength from 830 to 893 nm in increments of 0.25 nm. At each wavelength the output power of the laser is monitored and the interference fringes are recorded. The intensity of the interference fringes is normalized according to the power of the laser and the spectral response of the CCD detector. Figure 3 shows the normalized intensity envelope function after demodulation. The FWHM value is approximately 16.7 nm. According to the wavelength-to-depth

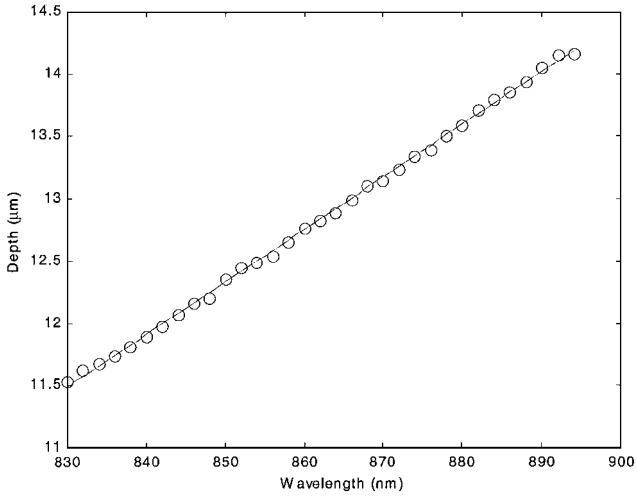

Fig. 2. Calibration for wavelength-to-depth encoding.

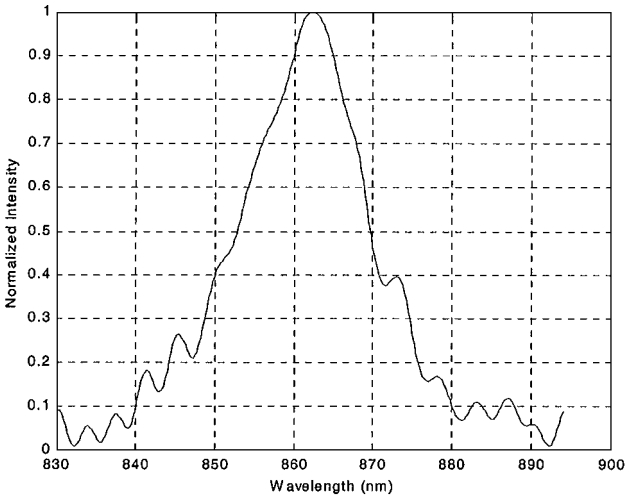

Fig. 3. Depth-response envelope with wavelength-to-depth scanning.

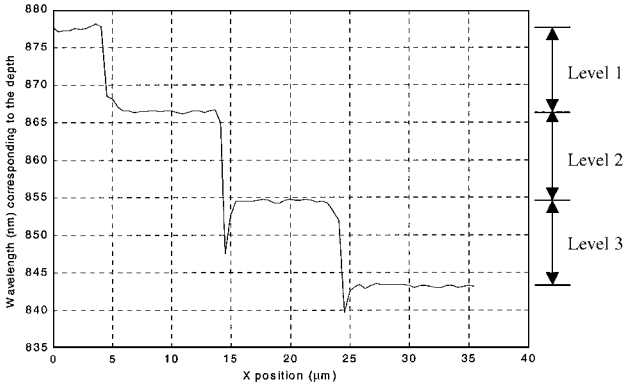

Fig. 4. Experimental results for a four-level grating.

Table 1. Comparison of Profile Measurements of a Four-Level Grating with a Dektak Profilometer and an Interference Microscope with Two Types of Scanning

	Interference Microscope		
Level (μm)	Wavelength-to-Depth	Mechanical	Dektak
1	0.471	0.469	0.457
2	0.504	0.462	0.483
3	0.481	0.498	0.450

calibration, this wavelength width corresponds to 0.71 μm in depth. For comparison we also measured the depth-discrimination capability of our system with mechanical scanning. The experimental FWHM value is ~0.70 μm. It can be seen that the longitudinal resolution of our system with wavelength-to-depth encoding is close to that with mechanical scanning.

For demonstration of quantitative profilometry measurement of 3D objects with high resolution, a four-level grating is used as the object for detection. The wavelength is also tuned from 830 to 894 nm in increments of 0.25 nm. According to the calibration result, each increment corresponds to a 0.0162-μm change in depth. The operational procedure is the same as in the depth-discrimination measurement. For each pixel the fringes are demodulated, and the amplitude envelope function is obtained. Then the wavelength corresponding to the center of mass of the envelope can be found. The depth of each level is obtained in terms of the wavelength-to-depth calibration. Figure 4 is the depth-section profile obtained with this technique. For comparison, we also measure the same object with a Dektak profilometer and with the same interference microscope but while scanning the object with a piezoelectric transducer. Table 1 lists the experimental results with the three different techniques. It can be seen from the table that the results obtained from the new technique are comparable with those obtained from the other two techniques.

In conclusion, a novel interference microscope based on a wavelength-to-depth encoding technique has been presented for high-resolution 3D imaging. In the system the object is scanned by use of a diffractive lens and wavelength tuning. Because we measure not the phase of the interference but only the occurrence of interference, the system is not affected much by vibrations. Recently, it was found that the switching time of a tunable distributed Bragg reflector laser can be as fast as a few nanoseconds.[15] Thus, with the rapid development of microfabrication and wavelength-tunable lasers, this technique is promising for fast, noncontact, high-resolution 3D imaging.

This work was supported by National Science Foundation. The authors are grateful to Fang Xu for offering the sample and to Sungdo Cha for discussions. G. Li is on leave from the Shanghai Institute of Optics and Fine Mechanics. His e-mail address is gqli@ece.ucsd.edu.

References

1. T. Wilson, ed., *Confocal Microscopy* (Academic, San Diego, Calif., 1990).
2. M. Gu and C. J. R. Sheppard, J. Opt. Soc. Am. A **11,** 1615 (1994).
3. G. Barbastathis, M. Balberg, and D. J. Brady, Opt. Lett. **24,** 813 (1999).
4. M. Davidson, K. Kaufman, I. Mazor, and F. Cohen, Proc. SPIE **775,** 233 (1987).
5. G. Kino and S. Chim, Appl. Opt. **29,** 3775 (1990).
6. F. C. Chang and G. Kino, Appl. Opt. **37,** 3471 (1998).
7. B. S. Lee and T. Strand, Appl. Opt. **29,** 3784 (1990).
8. T. Dresel, G. Hausler, and H. Venzke, Appl. Opt. **31,** 919 (1992).
9. P. J. Caber, Appl. Opt. **32,** 3438 (1993).
10. P. C. Sun and E. Arons, Appl. Opt. **34,** 1254 (1995).
11. A. Dubois, A. C. Boccara, and M. Lebec, Opt. Lett. **24,** 309 (1999).
12. L. Mandel and E. Wolf, *Optical Coherence and Quantum Optics* (Cambridge U. Press, New York, 1995), Chap. 4.
13. S. Dobson, P. C. Sun, and Y. Fainman, Appl. Opt. **36,** 4744 (1997).
14. J. W. Goodman, *Introduction to Fourier Optics* (McGraw-Hill, New York, 1996), Chaps. 5 and 6.
15. F. Delorme, G. Alibert, C. Ougier, S. Slempkes, and H. Nakajima, Electron. Lett. **34,** 279 (1998).